Composite Structures 93 (2011) 2375–2383

Contents lists available at ScienceDirect

Composite Structures

journal homepage: www.elsevier.com/locate/compstruct

Multi-scale modelling of sandwich structures using hierarchical kinematics

Q.Z. He [a], H. Hu [a,*], S. Belouettar [b], G. Guinta [b], K. Yu [a], Y. Liu [a], F. Biscani [b], E. Carrera [c], M. Potier-Ferry [d]

[a] School of Civil Engineering, Wuhan University, 8 South Road of East Lake, 430072 Wuhan, PR China
[b] Centre de Recherche Public Henri Tudor, 29, av. John F. Kennedy, L-1855 Luxembourg-Kirchberg, Luxembourg
[c] Politecnico di Torino, 24, c.so Duca degli Abruzzi, 10129 Turin, Italy
[d] LEM3, UMR CNRS 7239, Université Paul Verlaine-Metz, Ile du Saulcy, 57045 Metz Cedex 01, France

ARTICLE INFO

Article history:
Available online 3 April 2011

Keywords:
Multi-scale modelling
Arlequin
Hierarchical kinematics
Sandwich
Carrera's Unified Formulation

ABSTRACT

The aim of this paper is to present a multi-scale method for the mechanical modelling of sandwich structures. Low- and high-order sandwich elements are formulated on the basis of Carrera's Unified Formulation (CUF) and bridged within the Arlequin framework. According to CUF, an *N*-order polynomials approximation is assumed on the beam cross-section for the unknown displacements, being *N* a free parameter of the formulation. Low-order, computationally cheap elements are used to describe the global mechanical response. High-order, computationally demanding elements are used to capture the local effects in the boundary layers. CUF framework is here enhanced by the assumption of the Constrained Variational Principle (CVP) in order to derive a new class of layered beam finite elements with an independent kinematic field for each lamina. Results are assessed towards two- and three-dimensional finite element solutions. The numerical results show that, in the context of CUF, the Arlequin method effectively couples sub-domains modelled via variable order finite elements. The proposed coupled models yield accurate results, being able to predict both the global solution and the local effects, with a reduced computational cost.

1. Introduction

Due to their high specific strength- and stiffness-to-weight ratios, sandwich composite structures are widely used in many engineering applications, for instance, ships, automobiles, wind energy systems, bridge construction, satellites and aircrafts. A detailed understanding of their in-service behaviour, accounting also for damage is a relevant and challenging issue, see Belouettar et al. [1]. Adequate structural models should be, therefore, used. Accurate solutions, in general, entail a relevant amount of calculations on a finely discretised model of the structure. An approximation via three-dimensional finite elements is expensive, especially in the case of large structures. Results could be also unreliable, if a too high elements aspect-ratio is used.

Comprehensive reviews and assessments on the modelling of multi-layered and sandwich composites can be found, among the others, in the works by Carrera [2,3] and Hu et al. [4,5]. According to these reviews, layer-wise models, rather than the classical ones, should be used when an accurate prediction of transverse shear and normal stresses is required (see, also, Lekhnitskii [6]). The choice of the proper model might not be straightforward. The assumption of a new theory requires, in general, the derivation of new governing equations. This can be avoided by using Carrera's Unified Formulation (CUF), see Carrera [7], Carrera and Giunta [8–10] and Carrera et al. [11,12]. Within CUF, several kinematic assumptions for the displacement fields can be included hierarchically in one single formulation. This is particularly appealing since a very large variety of different theories can be implemented without any effort.

Over the last years, multi-scale modelling has evolved more and more. Nowadays, it represents one of the most interesting approaches for the modelling of the physical properties and the response of those complex materials and structures for which analyses should carried out at several scales (from the nano-scale up to the macro one). Among the others, the works by Curtin and Miller [13] and Liu et al. [14] are worth to be mentioned. As far as multi-scale structural modelling is concerned, several multi-scale approaches have been formulated. The Arlequin method by Ben Dhia and co-workers [15–18] or the so called bridging technique by Xiao and Belytschko [19] belong to a class of global/local methods. The literature presents several examples of its application to material science, see, for instance, Guidault and Belytschko [20], Prudhomme et al. [21] and Bauman et al. [22]. By means of an energy partition function and coupling operators, the Arlequin method allows the coupling of different physical states in order to perform multi-scale or multi-model simulations. An example is the superposition of refined local meshes to a coarse global one, allowing a multi-scale simulation in the sense of a locally refined targeted

* Corresponding author. Address: School of Civil Engineering, Wuhan University, 8 South Road of East Lake, 430072 Wuchang, PR China.
E-mail address: huheng@whu.edu.cn (H. Hu).

0263-8223/$ - see front matter © 2011 Elsevier Ltd. All rights reserved.
doi:10.1016/j.compstruct.2011.03.026

analysis. In Hu et al. [23], the Arlequin multi-scale framework was adopted for the linear static analysis of sandwich beams modelled via one- and two-dimensional finite elements. Several coupling operators were used in order to assess the proposed approach. The geometric non-linearities were accounted for in Hu et al. [24]. The non-linear governing equations were resolved via the Asymptotic Numerical Method, see Cochelin et al. [25] and Zahrouni et al. [26]. Very recently, the Arlequin method was formulated by Biscani et al. [27] in the context of CUF. Beam elements based on different kinematic assumptions were combined. Computational costs were reduced assuming refined models only in those zones with a quasi-three-dimensional stress field. As in Biscani et al. [27], in the present paper, low- and high-order sandwich beam finite elements are coupled via the Arlequin method in the framework of CUF. The novelty consists in the assumption of the Constrained Variational Principle in order to formulate a new class of layered beam finite elements with an independent kinematic field for each lamina. The linear static analysis of two- and three-dimensional sandwich beams is carried out. The proposed approach is validated towards two- and three-dimensional FEM results. Numerical investigation has shown that accurate results can be obtained with a significant reduction of the degrees of freedom of the model and, therefore, of the computational cost.

2. CUF framework for sandwich modelling

CUF framework is here enhanced by the assumption of the Constrained Variational Principle (CVP) in order to derive a new class of layered beam finite elements with an independent kinematic field for each lamina.

2.1. CUF kinematic field

In the CUF framework, several refined beam models can be systematically obtained considering the theory approximation order (N) as a free parameter of the formulation. The displacement field $\mathbf{u}$ is assumed as a linear combination of approximation function F_τ depending upon the y and z coordinates on the beams cross-section:

$$\mathbf{u} = F_\tau \mathbf{u}_\tau, \quad \tau = 1, 2, \ldots, N_p \tag{1}$$

$\mathbf{u}_\tau$ is the part of displacement vector that varies versus the axial coordinate x and N_p stands for the number of terms of the expansion. N is supposed to be an arbitrary number. Mac Laurin's polynomials are adopted as approximation or expansion functions. Table 1 presents N_p and F_τ as functions of N. According to Eq. (1), a second-order displacement field, for instance, is:

$$\begin{cases} u = u_1 + yu_2 + zu_3 + y^2u_4 + yzu_5 + z^2u_6 \\ v = v_1 + yv_2 + zv_3 + y^2v_4 + yzv_5 + z^2v_6 \\ w = w_1 + yw_2 + zw_3 + y^2w_4 + yzw_5 + z^2w_6 \end{cases} \tag{2}$$

For the sake of comparison to the two-dimensional modelling, a degenerated CUF theory is also considered: all the problem unknowns do not depend upon y coordinates. Displacement component v is disregarded. Under these hypotheses, a CUF second-order displacement field, for instance, reads:

Table 1
Mac Laurin's polynomials terms via Pascal's triangle.

N	N_u	F_τ
0	1	$F_1 = 1$
1	3	$F_2 = y$ $F_3 = z$
2	6	$F_4 = y^2$ $F_5 = yz$ $F_6 = z^2$
3	10	$F_7 = y^3$ $F_8 = y^2z$ $F_9 = yz^2$ $F_{10} = z^3$
...	...	...
N	$\frac{(N+1)(N+2)}{2}$	$F_{\frac{(N^2+N+2)}{2}} = y^N$ $F_{\frac{(N^2+N+4)}{2}} = y^{N-1}z \ldots$ $F_{\frac{N(N+3)}{2}} = yz^{N-1}$ $F_{\frac{(N+1)(N+2)}{2}} = z^N$

$$\begin{cases} u = u_1 + zu_2 + z^2u_3 \\ w = w_1 + zw_2 + z^2w_3 \end{cases} \tag{3}$$

2.2. Finite element modelling

The displacement vector $\mathbf{u}_\tau$ can be expressed in terms of shape functions ($\mathbf{N}_i$) and nodal unknowns ($\mathbf{q}_{\tau i}$):

$$\mathbf{u}_\tau = \mathbf{N}_i \mathbf{q}_{\tau i} \tag{4}$$

where:

$$\mathbf{q}_{\tau i} = \begin{Bmatrix} q_{x_{\tau i}} & q_{y_{\tau i}} & q_{z_{\tau i}} \end{Bmatrix}^T \tag{5}$$

and:

$$\mathbf{N}_i = \begin{bmatrix} N_{ui} & 0 & 0 \\ 0 & N_{vi} & 0 \\ 0 & 0 & N_{wi} \end{bmatrix} \tag{6}$$

T stands for vector transposition operator. In this work, N_{ui} are Lagrange's first-order interpolating polynomials. In order to enrich the displacement fields in width and height directions, N_{vi} and N_{wi} are Hermite's interpolating polynomials. By substituting Eq. (4) into Eq. (1), CUF approximation reads:

$$\mathbf{u} = F_\tau \mathbf{N}_i \mathbf{q}_{\tau i} \tag{7}$$

The element stiffness matrix can be obtained through the Principle of Virtual Displacement:

$$\delta \mathcal{P}^e = \delta L^e_{int} - \delta L^e_{ext} = 0 \tag{8}$$

where δ stands for virtual variation, L^e_{int} for the strain energy of a generic element and L^e_{ext} for the work of an external loading. By definition of strain energy:

$$\delta L^e_{int} = \int_{V^e} \delta \boldsymbol{\epsilon}^T \boldsymbol{\sigma} dV \tag{9}$$

where $\boldsymbol{\epsilon}$ and $\boldsymbol{\sigma}$ are the strain and stress vectors according to Voigt's notation. V^e is the element volume. In the case of small displacements, linear strains–displacements relations hold:

$$\boldsymbol{\epsilon} = \mathbf{L}\mathbf{u} \tag{10}$$

being $\mathbf{L}$ the following differential operator matrix:

$$\mathbf{L}^T = \begin{bmatrix} \frac{\partial}{\partial x} & 0 & 0 & 0 & \frac{\partial}{\partial z} & \frac{\partial}{\partial y} \\ 0 & \frac{\partial}{\partial y} & 0 & \frac{\partial}{\partial z} & 0 & \frac{\partial}{\partial x} \\ 0 & 0 & \frac{\partial}{\partial z} & \frac{\partial}{\partial y} & \frac{\partial}{\partial x} & 0 \end{bmatrix} \tag{11}$$

For a linear elastic material, Hooke's law holds:

$$\boldsymbol{\sigma} = \mathbf{D}\boldsymbol{\epsilon} \tag{12}$$

For sake of brevity, the explicit expression of the material stiffness matrix $\mathbf{D}$ is not here reported. It can be found in Reddy [28]. Considering Eqs. (7), (10) and (12), the virtual variation of the strain energy becomes:

$$\delta L^e_{int} = \delta \mathbf{q}^T_{\tau i} \int_{l^e} \int_{A^e} (F_\tau \mathbf{N}^T_i) \mathbf{L}^T \mathbf{D} \mathbf{L} (F_s \mathbf{N}_j) \, dA \, dx \, \mathbf{q}_{sj} \tag{13}$$

where $\mathbf{I}$ is the identity matrix and A^e and l^e the element cross-section and axial length, respectively. Indexes τ and s are related to the integrals of the expansion functions above the cross-section A^e, whereas indexes i and j are related to the integrals of the shape functions along the element axis. L^e_{int} in a compact form becomes:

$$\delta L^e_{int} = \delta \mathbf{q}^T_{\tau i} \mathbf{K}^{ij\tau s} \mathbf{q}_{sj} \tag{14}$$

where $\mathbf{K}^{ij\tau s} \in \mathbb{R}^{3\times 3}$ is the fundamental nucleo of the element stiffness matrix. It should be noted that no assumption on the approx-

imation order has been done. It is, therefore, possible to obtain a generic model without changing the formal expression of the nucleo. Once the approximation order N has been fixed, the actual element stiffness matrix is obtained via expansion versus indexes τ and s. Assembling the elements' stiffness matrices yields the global stiffness matrix $\mathbf{K}$. The strain energy of the whole beam in terms of $\mathbf{K}$ becomes:

$$\delta L_{int} = \{\delta \mathbf{Q}\}^T \mathbf{K} \{\mathbf{Q}\} \tag{15}$$

being $\{\mathbf{Q}\}$ the vector of the nodal displacements for the whole structure. The loading vector coherent to the model is derived for the case of a generic concentrated load $\mathbf{P}$ acting on the node i^* of coordinates (x_p, y_p, z_p):

$$\mathbf{P} = \{P_u \quad P_v \quad P_w\}^T \tag{16}$$

In this case, the virtual external work is:

$$\delta L^e_{ext} = \delta \mathbf{u}(x_p, y_p, z_p)^T \mathbf{P} \tag{17}$$

The fundamental nucleo of the load is obtained by means of the CUF approximation of the displacement field:

$$\delta L^e_{ext} = F_\tau \delta \mathbf{q}^T_{\tau i^*} \mathbf{P} \tag{18}$$

In the case of the whole structure, the previous equation reads:

$$\delta L_{ext} = \{\delta \mathbf{Q}\}^T \mathcal{F} \tag{19}$$

being $\mathcal{F}$ the vector of the nodal loads for the whole structure. Any other loading condition can be treated in a similar manner.

2.3. Application to sandwich structures

A three-dimensional sandwich beam with a soft core and stiff skins, as shown in Fig. 1, is considered. Beam geometry is such that h_f, h_c and h_{tot} are the thicknesses of the top and bottom faces, of the core and the total one. Beam z-axis is such that $-h_{tot}/2 \leqslant z \leqslant h_{tot}/2$. Beam's length and width are denoted by l and b, respectively. Subscripts t, b and c stand the top skin, bottom one and core, respectively. Thanks to CUF, the assumptions of no shear stress upon the top and bottom surfaces and no transverse deformation, used by many authors (see [5,23,29–31]), can be disregarded. The displacement field is considered independently for each layer. Congruency of the displacement field at layers interface is ensured via the Constrained Variational Principle (CVP). For the beam shown in Fig. 1, the following additional constraining relations are accounted for:

$$\begin{cases} \boldsymbol{B}_1(\boldsymbol{u}_t, \boldsymbol{u}_c) = \boldsymbol{u}_t|_{z=h_c/2} - \boldsymbol{u}_c|_{z=h_c/2} = \mathbf{0} \\ \boldsymbol{B}_2(\boldsymbol{u}_b, \boldsymbol{u}_c) = \boldsymbol{u}_b|_{z=-h_c/2} - \boldsymbol{u}_c|_{z=-h_c/2} = \mathbf{0} \end{cases} \tag{20}$$

where $\boldsymbol{B}_1$ denotes the continuity condition between the top face and the core and $\boldsymbol{B_2}$ stands for the bottom face-core one. By introducing Lagrange's multipliers μ_1 and μ_2 as fictitious gluing forces on the interfaces, the weak form of Eq. (20) reads:

$$\begin{cases} \int_{\Gamma_1} \boldsymbol{\mu}_1 \boldsymbol{B}_1 d\Gamma = \boldsymbol{0}, \quad \Gamma_1 = \{(x,y,z) : x \in [0,L], \\ \quad y \in [-b/2, b/2], z = h_c/2\} \\ \int_{\Gamma_2} \boldsymbol{\mu}_2 \boldsymbol{B}_2 d\Gamma = \boldsymbol{0}, \quad \Gamma_2 = \{(x,y,z) : x \in [0,L], \\ \quad y \in [-b/2, b/2], z = -h_c/2\} \end{cases} \tag{21}$$

Eq. (21) could be considered as a constraint in an optimisation problem, and the corresponding functional is:

$$\delta \mathcal{P}^{e*} = \delta \mathcal{P}^e_t + \delta \mathcal{P}^e_c + \delta \mathcal{P}^e_b + \delta \int_{\Gamma^e_\zeta} \boldsymbol{\mu}_\zeta \boldsymbol{B}_\zeta d\Gamma, \quad \zeta = 1,2 \tag{22}$$

where $\delta \mathcal{P}^e$ has been defined in Eq. (8), ζ is a dummy index for summation over the laminate interfaces and the interfaces boundaries Γ^e_1 and Γ^e_2 can be expressed as:

$$\begin{cases} \Gamma^e_1 = \{(x,y,z) : x \in [x^e_0, x^e_1], \ y \in [-b/2, b/2], \ z = h_c/2\} \\ \Gamma^e_2 = \{(x,y,z) : x \in [x^e_0, x^e_1], \ y \in [-b/2, b/2], \ z = -h_c/2\} \end{cases} \tag{23}$$

being x^e_0 and x^e_1 the axial coordinates of the element external nodes. $\boldsymbol{\mu}_\zeta$ are discretised according to CUF framework:

$$\boldsymbol{\mu}_\zeta = F_{\tau_{\mu\zeta}} \mathbf{N}_{i_\zeta} \mathbf{q}_{\tau_{\mu\zeta} i_\zeta} \tag{24}$$

The approximation order of Lagrange's multipliers is a free parameter and it can be properly chosen to obtain an efficient solution. In what follows, term $\int_{\Gamma^e_1} \boldsymbol{\mu}_1 \delta \boldsymbol{B}_1 d\Gamma$ in Eq. (22) is derived according to CUF. All the other terms can be obtained in a similar manner.

$$\begin{aligned} \int_{\Gamma^e_1} \delta \boldsymbol{\mu}_1 \boldsymbol{B}_1 d\Gamma &= \delta \mathbf{q}^T_{\tau_{\mu1} i_1} \int_{\Gamma^e_1} F_{\tau_{\mu1}} F_{s_t} \mathbf{N}^T_{i_1} \mathbf{N}_j d\Gamma \mathbf{q}_{s_t j} \\ &\quad - \delta \mathbf{q}^T_{\tau_{\mu1} i_1} \int_{\Gamma^e_1} F_{\tau_{\mu1}} F_{s_c} \mathbf{N}^T_{i_1} \mathbf{N}_j d\Gamma \mathbf{q}_{s_c j} \\ &= \delta \mathbf{q}^T_{\tau_{\mu1} i_1} \mathbf{B}^{i_1 j \tau_{\mu1} s_t}_{1t} \mathbf{q}_{s_t j} - \delta \mathbf{q}^T_{\tau_{\mu1} i_1} \mathbf{B}^{i_1 j \tau_{\mu1} s_c}_{1c} \mathbf{q}_{s_c j} \end{aligned} \tag{25}$$

where:

$$\begin{cases} \mathbf{B}^{i_1 j \tau_{\mu1} s_t}_{1t} = \int_{\Gamma^e_1} F_{\tau_{\mu1}} F_{s_t} \mathbf{N}^T_{i_1} \mathbf{N}_j d\Gamma \\ \mathbf{B}^{i_1 j \tau_{\mu1} s_c}_{1c} = \int_{\Gamma^e_1} F_{\tau_{\mu1}} F_{s_c} \mathbf{N}^T_{i_1} \mathbf{N}_j d\Gamma \end{cases} \tag{26}$$

For the whole structure:

$$\int_{\cup \Gamma^e_1} \delta \boldsymbol{\mu}_1 \boldsymbol{B}_1 d\Gamma = \left\{\delta \mathbf{Q}_{\mu1}\right\}^T \boldsymbol{\mathcal{B}}_{1t} \{\mathbf{Q}_t\} - \left\{\delta \mathbf{Q}_{\mu1}\right\}^T \boldsymbol{\mathcal{B}}_{1c} \{\mathbf{Q}_c\} \tag{27}$$

Interface stress continuity can be imposed via CVP in a similar manner. The linear algebraic governing equations for the whole beam are obtained assembling the derived stiffness and constraining matrices:

$$\begin{bmatrix} \boldsymbol{K}_t & \mathbf{0} & \mathbf{0} & \boldsymbol{\mathcal{B}}^T_{1t} & \mathbf{0} \\ \mathbf{0} & \boldsymbol{K}_c & \mathbf{0} & -\boldsymbol{\mathcal{B}}^T_{1c} & -\boldsymbol{\mathcal{B}}^T_{2c} \\ \mathbf{0} & \mathbf{0} & \boldsymbol{K}_b & \mathbf{0} & \boldsymbol{\mathcal{B}}^T_{2b} \\ \boldsymbol{\mathcal{B}}_{1t} & -\boldsymbol{\mathcal{B}}_{1c} & \mathbf{0} & \mathbf{0} & \mathbf{0} \\ \mathbf{0} & -\boldsymbol{\mathcal{B}}_{2c} & \boldsymbol{\mathcal{B}}_{2b} & \mathbf{0} & \mathbf{0} \end{bmatrix} \begin{bmatrix} \mathbf{Q}_t \\ \mathbf{Q}_c \\ \mathbf{Q}_b \\ \mathbf{Q}_{\mu1} \\ \mathbf{Q}_{\mu2} \end{bmatrix} = \begin{bmatrix} \mathcal{F}_t \\ \mathcal{F}_c \\ \mathcal{F}_b \\ \mathbf{0} \\ \mathbf{0} \end{bmatrix} \tag{28}$$

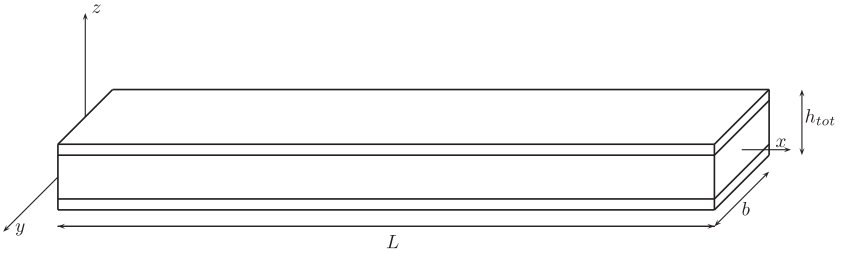

Fig. 1. Sketch of a sandwich beam.

3. Bridging technique

In order to improve the computational efficiency, a bridging technique is adopted. In this section, the Arlequin method is derived within the CUF framework.

3.1. Arlequin method

According to the Arlequin framework, the beam volume V is partitioned into two overlapping sub-domains (see Fig. 2) V_r in which a refined model is considered and V_c where a coarse (or low-order) model is assumed. The intersecting volume constitutes the superposition zone $V_s = V_r \cap V_c$. Subscripts r and c stand for refined and coarse sub-domain, respectively. For a generic element of a sub-domain V_k, the internal and external virtual works are:

$$\begin{cases} \delta L_{int}^{ek}(\boldsymbol{u}_k) = \int_{V_k^e} \alpha_k \delta\boldsymbol{\epsilon}^T(\boldsymbol{u}_k)\boldsymbol{\sigma}(\boldsymbol{u}_k)dV \\ \delta L_{ext}^{ek}(\boldsymbol{u}_k) = \int_{V_k^e} \beta_k \delta\boldsymbol{u}_k^T \boldsymbol{f}_k dV \end{cases} \text{with } k = r \text{ or } c \tag{29}$$

where $\boldsymbol{u}_k$, $\delta\boldsymbol{u}_k$ and $\boldsymbol{f}_k$ are the displacement, the virtual displacement and the external force for an element in V_k (V_r or V_c). To avoid considering the energy of the total system in the coupling zone twice, the energy associated to each zone is balanced by the weighting functions α_k, for the internal work, and β_k for the external work. They should satisfy the following equalities:

$$\begin{cases} \alpha_k = \beta_k = 1 & \text{in } V_k \setminus V_s \text{ with } k = r \text{ or } c \\ \alpha_r + \alpha_c = \beta_r + \beta_c = 1 & \text{in } V_s \end{cases} \tag{30}$$

The effect of α_k and β_k on the solution has been extensively investigated in Ben Dhia [16], Ben Dhia and Rateau [18] and in Hu et al. [23]. Their influence, therefore, is not here investigated. According to those works, α_k and β_k should be such that the V_r has a higher weight than V_c in the global equilibrium. They are assumed to be the positive piecewise functions in V_s such that $\alpha_r = \beta_r = 0.98$ and, consequently, $\alpha_c = \beta_c = 0.02$. Refined and coarse models are coupled considering that the mechanical state in V_s of the two model should be identical in a mean sense:

$$\boldsymbol{u}_r - \boldsymbol{u}_c = 0, \quad \forall (x,y,z) \in V_s^e. \tag{31}$$

$\boldsymbol{u}_c$ and $\boldsymbol{u}_r$ represent here displacement fields, but, in a broad sense, they can be seen as generic mechanical fields. By introducing Lagrange's multipliers:

$$\boldsymbol{\lambda} = \{\lambda_u \ \lambda_v \ \lambda_w\}^T \tag{32}$$

as a fictive gluing force, Eq. (31) is rewritten in a weak form:

$$\mathcal{C}^e(\boldsymbol{u}_r - \boldsymbol{u}_c, \boldsymbol{\lambda}) = 0, \quad \forall \boldsymbol{\lambda} \in M, \quad \forall (x,y,z) \in V_s^e. \tag{33}$$

where M is a mediator space and $\mathcal{C}^e$ is a coupling operator.

$$\mathcal{C}^e(\boldsymbol{\lambda}, \boldsymbol{u}_k) = \int_{V_s^e} \left[\boldsymbol{\lambda}^T \boldsymbol{u}_k + \ell^2 \boldsymbol{\epsilon}(\boldsymbol{\lambda})^T \boldsymbol{\epsilon}(\boldsymbol{u}_k)\right] dV \text{ with } k = r \text{ or } c \tag{34}$$

In literature there exist several coupling operators, the one addressed in Eq. (34) is know as H^1-type coupling operator where ℓ is a real parameter homogeneous to a length. In the case of $\ell = 0$, the L^2-type coupling operator is obtained. It has been shown by Ben Dhia and Rateau [18] that the H^1-type coupling operator introduces less perturbations in the solution in the coupling zone. That result was confirmed by the comparative investigation of the two coupling operators in Biscani et al. [27] and Bauman et al. [32]. In the present work, therefore, only H^1-type coupling operator with $\ell = L_c$ will be accounted for.

$\boldsymbol{\epsilon}(\boldsymbol{\lambda})$ is defined in the same manner as the mechanical strain $\boldsymbol{\epsilon}(bi\ u_k)$ where the Lagrangian multiplier field is used instead of the displacement one. Eq. (33) could be considered as a constraint in an optimization problem. In this manner, the virtual work equation assumes the following form:

$$\delta\mathcal{P}_k^e(\boldsymbol{u}_k) + \delta\mathcal{C}^e(\boldsymbol{u}_r - \boldsymbol{u}_c, \boldsymbol{\lambda}) = 0, \quad k = r, c \quad \forall\delta\boldsymbol{u}_k \in K.A., \forall\delta\boldsymbol{\lambda} \in M \tag{35}$$

where *K.A.* stands for kinematically admissible and:

$$\delta\mathcal{P}_k^e(\boldsymbol{u}_k) = \delta L_{int}^{ek}(\boldsymbol{u}_k) - \delta L_{ext}^{ek}(\boldsymbol{u}_k) \tag{36}$$

Three governing equations can be obtained from Eq. (35):

$$\begin{cases} \delta\mathcal{P}_r^e(\boldsymbol{u}_r) + \mathcal{C}^e(\delta\boldsymbol{u}_r, \boldsymbol{\lambda}) = 0 & \forall\delta\boldsymbol{u}_r \in K.A., \\ \delta\mathcal{P}_c^e(\boldsymbol{u}_c) - \mathcal{C}^e(\delta\boldsymbol{u}_c, \boldsymbol{\lambda}) = 0 & \forall\delta\boldsymbol{u}_c \in K.A., \\ \mathcal{C}^e(\delta\boldsymbol{\lambda}, \boldsymbol{u}_r) - \mathcal{C}^e(\delta\boldsymbol{\lambda}, \boldsymbol{u}_c) = 0 & \forall\delta\boldsymbol{\lambda} \in M \end{cases} \tag{37}$$

The finite element method is used to solve Eq. (37). According to CUF framework, the discretisation of the unknowns has the following form:

$$\boldsymbol{u}_k = \{u_k \quad v_k \quad w_k\}^T = F_{\tau_k} \mathbf{N}_{i_k} \mathbf{q}_{\tau_k i_k} \quad k = r \text{ or } c \tag{38}$$

$$\boldsymbol{\lambda} = \{\lambda_u \quad \lambda_v \quad \lambda_w\}^T = F_{\tau_\lambda} \mathbf{N}_{i_\lambda} \mathbf{q}_{\tau_\lambda i_\lambda} \tag{39}$$

where $\mathbf{q}_{\tau_r i_r}$, $\mathbf{q}_{\tau_c i_c}$ and $\mathbf{q}_{\tau_\lambda i_\lambda}$ are the elementary nodal unknowns of $\boldsymbol{u}_r$, $\boldsymbol{u}_c$ and $\boldsymbol{\lambda}$. For each sub-domain a different expansion order along the cross-section is considered. In order to avoid locking and according to Ben Dhia and Rateau [18], the same expansion order is used for $\boldsymbol{u}_c$ and $\boldsymbol{\lambda}$. The coupling operator in Eq. (34) becomes:

$$\mathcal{C}^e(\mathbf{q}_{\tau_\lambda i_\lambda}, \mathbf{q}_{s_k j_k}) = \mathbf{q}_{\tau_\lambda i_\lambda}^T \int_{V_s^e} \left[F_{\tau_\lambda} F_{s_k} \mathbf{N}_{i_\lambda}^T \mathbf{N}_{j_k} + \ell^2 \left(F_{\tau_\lambda} \mathbf{N}_{i_\lambda}^T\right) \mathbf{L}^T \mathbf{L} \left(F_{s_k} \mathbf{N}_{j_k}\right)\right] dV \mathbf{q}_{s_k j_k}$$
$$\text{with} k = r \text{ or } c \tag{40}$$

The previous equation yields the coupling matrices $\mathbf{C}^{i_\lambda j_k \tau_\lambda s_k}$ at element level:

$$\mathbf{C}^{i_\lambda j_k \tau_\lambda s_k} = \int_{V_s^e} \left[F_{\tau_\lambda} F_{s_k} \mathbf{N}_{i_\lambda}^T \mathbf{N}_{j_k} + \ell^2 \left(F_{\tau_\lambda} \mathbf{N}_{i_\lambda}^T\right) \mathbf{L}^T \mathbf{L} \left(F_{s_k} \mathbf{N}_{j_k}\right)\right] dV \text{ with } k = r \text{ or } c \tag{41}$$

Coupling matrix of L^2 coupling operator can be obtained as particular case of Eq. (41) with $\ell = 0$. The linear governing equations for the whole beam are:

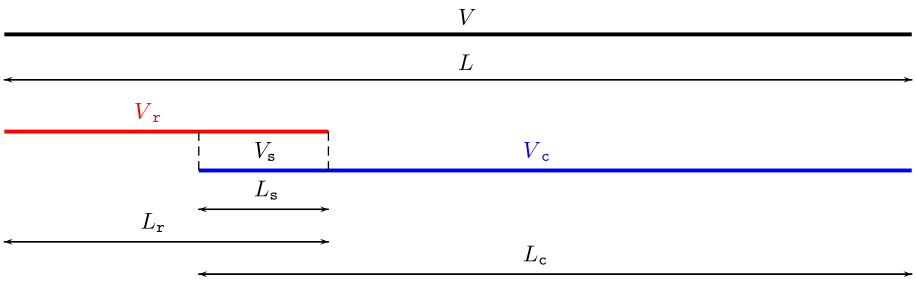

Fig. 2. Beam division according to the Arlequin method.

$$\begin{bmatrix} \boldsymbol{K}_{\mathrm{r}} & \mathbf{0} & \mathcal{C}_{\mathrm{r}}^{T} \\ \mathbf{0} & \boldsymbol{K}_{\mathrm{c}} & -\mathcal{C}_{\mathrm{c}}^{T} \\ \mathcal{C}_{\mathrm{r}} & -\mathcal{C}_{\mathrm{c}} & \mathbf{0} \end{bmatrix} \begin{bmatrix} \boldsymbol{Q}_{\mathrm{r}} \\ \boldsymbol{Q}_{\mathrm{c}} \\ \boldsymbol{Q}_{\lambda} \end{bmatrix} = \begin{bmatrix} \mathcal{F}_{\mathrm{r}} \\ \mathcal{F}_{\mathrm{c}} \\ \mathbf{0} \end{bmatrix} \tag{42}$$

where $\boldsymbol{K}_{\mathrm{r}}$ and $\boldsymbol{K}_{\mathrm{c}}$ have been defined in Eq. (15) and $\mathcal{F}_{\mathrm{r}}$ and F_{c} in Eq. (19). $\boldsymbol{Q}_{\mathrm{r}}$ and $\boldsymbol{Q}_{\mathrm{c}}$ are the global degrees of freedom in the refined sub-domain and in the course one. $\boldsymbol{Q}_{\lambda}$ are the degrees of freedom of Lagrange multiplier in the coupling domain. $\mathcal{C}_{\mathrm{k}}$ are obtained from its nucleo as expressed in Eq. (41) and via assembling over the whole elements in the coupling zone.

3.2. Application to CUF sandwich models

The Arlequin method is now applied to the sandwich beams. It should be emphasised that the coupling zone involves three layers, that is, each layer is approximated via both refined and coarse models that overlap each other. For instance, the displacement field $\boldsymbol{u}_t$ is divided into a refined model $\boldsymbol{u}_{tr}$ and a coarse one $\boldsymbol{u}_{tc}$. The constraining conditions in Eq. (20) have to be rewritten in order to account for both V_{r} and V_{c}:

$$\begin{cases} \boldsymbol{B}_1 = \boldsymbol{B}_{1\mathrm{r}} + \boldsymbol{B}_{1\mathrm{c}} = (\boldsymbol{u}_{\mathrm{tr}}|_{z=h_c/2} - \boldsymbol{u}_{\mathrm{cr}}|_{z=h_c/2}) \\ \quad +(\boldsymbol{u}_{\mathrm{tc}}|_{z=h_c/2} - \boldsymbol{u}_{\mathrm{cc}}|_{z=h_c/2}) = \mathbf{0} \\ \boldsymbol{B}_2 = \boldsymbol{B}_{2\mathrm{r}} + \boldsymbol{B}_{2\mathrm{c}} = (\boldsymbol{u}_{\mathrm{tr}}|_{z=-h_c/2} - \boldsymbol{u}_{\mathrm{cr}}|_{z=-h_c/2}) \\ \quad +(\boldsymbol{u}_{\mathrm{tc}}|_{z=-h_c/2} - \boldsymbol{u}_{\mathrm{cc}}|_{z=-h_c/2}) = \mathbf{0} \end{cases} \tag{43}$$

The interfaces boundaries in Eq. (23) can be rewritten as:

$$\begin{cases} \Gamma_1^e = \Gamma_{1\mathrm{r}}^e \cup \Gamma_{1\mathrm{c}}^e \\ \Gamma_2^e = \Gamma_{2\mathrm{r}}^e \cup \Gamma_{2\mathrm{c}}^e \end{cases} \tag{44}$$

As previously done, only the term $\int_{\Gamma_1^e} \boldsymbol{\mu}_1 \delta^e B_1 d\Gamma$ is explicitly derived. Considering the first of Eqs. (44), (25) now reads:

$$\int_{\Gamma_1^e} \boldsymbol{\mu}_1 \delta \boldsymbol{B}_1 d\Gamma = \int_{\Gamma_{1\mathrm{r}^e}} \boldsymbol{\mu}_{1\mathrm{r}} \delta \boldsymbol{B}_{1\mathrm{r}} d\Gamma + \int_{\Gamma_{1\mathrm{c}^e}} \boldsymbol{\mu}_{1\mathrm{c}} \delta \boldsymbol{B}_{1\mathrm{c}} d\Gamma \tag{45}$$

Via substitution of the new constraining conditions and of the CUF approximation of Lagrange multipliers $\boldsymbol{\mu}_{1\mathrm{r}}$ and $\boldsymbol{\mu}_{1\mathrm{c}}$, the previous equation becomes:

$$\begin{aligned} \int_{\Gamma_1^e} \boldsymbol{\mu}_1 \delta \boldsymbol{B}_1 d\Gamma = {} & \delta \mathbf{q}_{\tau_{\mu 1\mathrm{r}} i_{1\mathrm{r}}}^{T} \left(\mathbf{B}_{1\mathrm{tr}}^{i_{1\mathrm{r}} j_{\mathrm{r}} \tau_{\mu 1\mathrm{r}} s_{\mathrm{tr}}} \mathbf{q}_{s_{\mathrm{tr}} j_{\mathrm{r}}} - \mathbf{B}_{1\mathrm{cr}}^{i_{1\mathrm{r}} j_{\mathrm{r}} \tau_{\mu 1\mathrm{r}} s_{\mathrm{cr}}} \mathbf{q}_{s_{\mathrm{cr}} j_{\mathrm{r}}} \right) \\ & + \delta \mathbf{q}_{\tau_{\mu 1\mathrm{c}} i_{1\mathrm{c}}}^{T} \left(\mathbf{B}_{1\mathrm{tc}}^{i_{1\mathrm{c}} j_{\mathrm{c}} \tau_{\mu 1\mathrm{c}} s_{\mathrm{tc}}} \mathbf{q}_{s_{\mathrm{tc}} j_{\mathrm{c}}} - \mathbf{B}_{1\mathrm{cc}}^{i_{1\mathrm{c}} j_{\mathrm{c}} \tau_{\mu 1\mathrm{c}} s_{\mathrm{cc}}} \mathbf{q}_{s_{\mathrm{cc}} j_{\mathrm{c}}} \right) \end{aligned} \tag{46}$$

For the whole beam:

$$\begin{aligned} \int_{\cup \Gamma_1^e} \delta \boldsymbol{\mu}_1 \boldsymbol{B}_1 d\Gamma = {} & \left\{ \delta \mathbf{Q}_{\mu 1\mathrm{r}} \right\}^{T} \left(\mathcal{B}_{1\mathrm{tr}} \{ \mathbf{Q}_{\mathrm{tr}} \} - \mathcal{B}_{1\mathrm{cr}} \{ \mathbf{Q}_{\mathrm{cr}} \} \right) \\ & + \left\{ \delta \mathbf{Q}_{\mu 1\mathrm{c}} \right\}^{T} \left(\mathcal{B}_{1\mathrm{tc}} \{ \mathbf{Q}_{\mathrm{tc}} \} - \mathcal{B}_{1\mathrm{cc}} \{ \mathbf{Q}_{\mathrm{cc}} \} \right) \end{aligned} \tag{47}$$

The governing equations at element level are obtained characterising Eq. (35) for the top and bottom skins and for the core. The global governing equations are:

$$[\overline{\boldsymbol{K}}] \left\{ \overline{\mathbf{Q}} \right\} = \{ \overline{\mathcal{F}} \} \tag{48}$$

where:

$$[\overline{\boldsymbol{K}}] = \begin{bmatrix} \boldsymbol{K}_{tr} & \mathbf{0} & \mathcal{C}_{tr}^{T} & \mathbf{0} & \mathbf{0} & \mathbf{0} & \mathbf{0} & \mathbf{0} & \mathbf{0} & \mathcal{B}_{1tr^T} & \mathbf{0} & \mathbf{0} & \mathbf{0} \\ \mathbf{0} & \boldsymbol{K}_{tc} & -\mathcal{C}_{tc}^{T} & \mathbf{0} & \mathbf{0} & \mathbf{0} & \mathbf{0} & \mathbf{0} & \mathbf{0} & \mathbf{0} & \mathcal{B}_{1tc^T} & \mathbf{0} & \mathbf{0} \\ \mathcal{C}_{tr} & -\mathcal{C}_{tc} & \mathbf{0} & \mathbf{0} & \mathbf{0} & \mathbf{0} & \mathbf{0} & \mathbf{0} & \mathbf{0} & \mathbf{0} & \mathbf{0} & \mathbf{0} & \mathbf{0} \\ \mathbf{0} & \mathbf{0} & \mathbf{0} & \boldsymbol{K}_{cr} & \mathbf{0} & \mathcal{C}_{cr}^{T} & \mathbf{0} & \mathbf{0} & \mathbf{0} & -\mathcal{B}_{1cr}^{T} & \mathbf{0} & -\mathcal{B}_{2cr}^{T} & \mathbf{0} \\ \mathbf{0} & \mathbf{0} & \mathbf{0} & \mathbf{0} & \boldsymbol{K}_{cc} & -\mathcal{C}_{cc}^{T} & \mathbf{0} & \mathbf{0} & \mathbf{0} & \mathbf{0} & -\mathcal{B}_{1cc}^{T} & \mathbf{0} & -\mathcal{B}_{2cc}^{T} \\ \mathbf{0} & \mathbf{0} & \mathbf{0} & \mathcal{C}_{cr} & -\mathcal{C}_{cc} & \mathbf{0} & \mathbf{0} & \mathbf{0} & \mathbf{0} & \mathbf{0} & \mathbf{0} & \mathbf{0} & \mathbf{0} \\ \mathbf{0} & \mathbf{0} & \mathbf{0} & \mathbf{0} & \mathbf{0} & \mathbf{0} & \boldsymbol{K}_{br} & \mathbf{0} & \mathcal{C}_{br}^{T} & \mathbf{0} & \mathbf{0} & \mathcal{B}_{2br}^{T} & \mathbf{0} \\ \mathbf{0} & \mathbf{0} & \mathbf{0} & \mathbf{0} & \mathbf{0} & \mathbf{0} & \mathbf{0} & \boldsymbol{K}_{bc} & -\mathcal{C}_{bc}^{T} & \mathbf{0} & \mathbf{0} & \mathbf{0} & \mathcal{B}_{2bc}^{T} \\ \mathbf{0} & \mathbf{0} & \mathbf{0} & \mathbf{0} & \mathbf{0} & \mathbf{0} & \mathcal{C}_{br} & -\mathcal{C}_{bc} & \mathbf{0} & \mathbf{0} & \mathbf{0} & \mathbf{0} & \mathbf{0} \\ \mathcal{B}_{1tr} & \mathbf{0} & \mathbf{0} & -\mathcal{B}_{1cr} & \mathbf{0} & \mathbf{0} & \mathbf{0} & \mathbf{0} & \mathbf{0} & \mathbf{0} & \mathbf{0} & \mathbf{0} & \mathbf{0} \\ \mathbf{0} & \mathcal{B}_{1tc} & \mathbf{0} & \mathbf{0} & -\mathcal{B}_{1cc} & \mathbf{0} & \mathbf{0} & \mathbf{0} & \mathbf{0} & \mathbf{0} & \mathbf{0} & \mathbf{0} & \mathbf{0} \\ \mathbf{0} & \mathbf{0} & \mathbf{0} & -\mathcal{B}_{2cr} & \mathbf{0} & \mathbf{0} & \mathcal{B}_{2br} & \mathbf{0} & \mathbf{0} & \mathbf{0} & \mathbf{0} & \mathbf{0} & \mathbf{0} \\ \mathbf{0} & \mathbf{0} & \mathbf{0} & \mathbf{0} & -\mathcal{B}_{2cc} & \mathbf{0} & \mathbf{0} & \mathcal{B}_{2bc} & \mathbf{0} & \mathbf{0} & \mathbf{0} & \mathbf{0} & \mathbf{0} \end{bmatrix} \tag{49}$$

$$\left\{ \overline{\mathbf{Q}} \right\} = \{ \mathbf{Q}_{\mathrm{tr}} \quad \mathbf{Q}_{\mathrm{tc}} \quad \mathbf{Q}_{\lambda} \quad \mathbf{Q}_{\mathrm{cr}} \quad \mathbf{Q}_{\mathrm{cc}} \quad \mathbf{Q}_{\lambda} \quad \mathbf{Q}_{\mathrm{br}} \quad \mathbf{Q}_{\mathrm{bc}} \quad \mathbf{Q}_{\lambda} \quad \mathbf{Q}_{\mu 1\mathrm{r}} \quad \mathbf{Q}_{\mu 1\mathrm{c}} \quad \mathbf{Q}_{\mu 2\mathrm{r}} \quad \mathbf{Q}_{\mu 2\mathrm{c}} \}^{T} \tag{50}$$

$$\{ \overline{\mathcal{F}} \} = \{ \mathcal{F}_{tr} \quad \mathcal{F}_{tc} \quad \mathbf{0} \quad \mathcal{F}_{cr} \quad \mathcal{F}_{cc} \quad \mathbf{0} \quad \mathcal{F}_{br} \quad \mathcal{F}_{bc} \quad \mathbf{0} \quad \mathbf{0} \quad \mathbf{0} \quad \mathbf{0} \quad \mathbf{0} \} \tag{51}$$

4. Numerical results

After validation of the proposed mono-model solutions, the effectiveness of the application of the Arlequin method with the CUF framework is investigated. Two- and three-dimensional beam models are investigated. Two-dimensional models are assessed towards two-dimensional (2D) FEM solutions using quadratic eight-node elements. A three-dimensional FEM model has been developed via the commercial code ANSYS to validate the proposed three-dimensional results.

4.1. Validation of CUF sandwich mono-model beam elements

A 3-point bending sandwich beam loaded as shown in Fig. 3 is investigated. Beam geometry, material properties and load amplitude are presented in Table 2. The core-to-face Young's modulus ratio E_c/E_f is as low as 10^{-4} and as high as 1. Beam mechanics is described in terms of transverse displacement $\bar{w} = w(L/2, 0)$, shear stress component $\bar{\tau}_{xz} = \tau_{xz}(L/4, 0)$ and normal stress component $\bar{\sigma}_{xx} = \sigma_{xx}(L/2, h_{tot}/2)$. Results are presented in Table 3. A second-order CUF sandwich model yields results that match the reference FEM 2D solution for all the considered values of E_c/E_f. Increasing

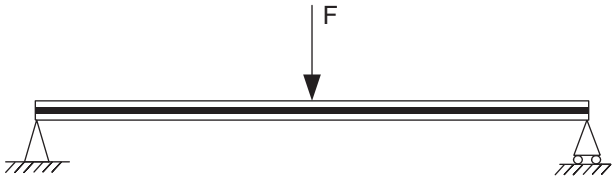

Fig. 3. 3-Point bending sandwich beam.

Table 2
Parameters of the simply supported sandwich beam.

E_f (MPa)	ν_f, ν_c	L (m)	h_{tot} (m)	h_c/h_f	F (N/m)
69,000	0.3	0.5	0.01	1	100

Table 3
Validation of sandwich CUF mono-model.

		FEM 2D	$N=2$	$N=3$	$N=4$
$\frac{E_c}{E_f}=1$	$-10^5\cdot\bar{w}$ (m)	4.53	4.53	4.53	4.53
	$-10^{-3}\cdot\bar{\tau}_{xz}$ (Pa)	7.64	7.40	7.40	7.65
	$-10^{-5}\cdot\bar{\sigma}_{xx}$ (Pa)	3.75	3.75	3.75	3.75
$\frac{E_c}{E_f}=10^{-1}$	$-10^5\cdot\bar{w}$ (m)	4.72	4.72	4.72	4.72
	$-10^{-3}\cdot t\bar{a}u_{xz}$ (Pa)	7.00	6.98	7.01	7.01
	$-10^{-5}\cdot\bar{\sigma}_{xx}$ (Pa)	3.88	3.88	3.88	3.88
$\frac{E_c}{E_f}=10^{-2}$	$-10^5\cdot\bar{w}$ (m)	4.99	4.99	5.00	5.00
	$-10^{-3}\cdot t\bar{a}u_{xz}$ (Pa)	6.93	6.93	6.93	6.94
	$-10^{-5}\cdot\bar{\sigma}_{xx}$ (Pa)	3.89	3.89	3.89	3.89
$\frac{E_c}{E_f}=10^{-3}$	$-10^5\cdot\bar{w}$ (m)	7.32	7.34	7.35	7.36
	$-10^{-3}\cdot\bar{\tau}_{xz}$ (Pa)	6.79	6.75	6.76	6.76
	$-10^{-5}\cdot\bar{\sigma}_{xx}$ (Pa)	3.98	3.97	3.97	3.97
$\frac{E_c}{E_f}=10^{-4}$	$-10^4\cdot\bar{w}$ (m)	2.24	2.26	2.27	2.29
	$-10^{-3}\cdot\bar{\tau}_{xz}$ (Pa)	4.64	4.61	4.61	4.61
	$-10^{-5}\cdot\bar{\sigma}_{xx}$ (Pa)	6.92	6.87	6.87	6.86

the expansion order, the solution converges. When E_c/E_f ranges from 10^{-3} to 10^{-4}, a great variation of $\bar{\sigma}_{xx}$ is observed.

4.2. Two-dimensional CUF sandwich multi-model analysis

A cantilever beam (as shown in Fig. 4) is considered. Table 4 presents the mechanical properties, the geometrical data and the load amplitude. A relatively short beam ($L/h_{tot}=20$) is investigated. The refined model is used in the neighbourhood of the loading application area. V_c is modelled via 36 elements based on a second-order model ($N_c=2$), whereas 24 fourth-order elements are used for V_r. In the superposition zone, elements differ for both expansion order and length. Due to the geometric and material configurations (relatively short beam with soft core and stiff faces) and the loading (localised force), transverse shear deformation and zig-zag variation above the cross-section are expected to play an important role in the mechanics of the beam. Results are assessed towards a FEM model based on Q8 plate elements. Figs. 5 and 6

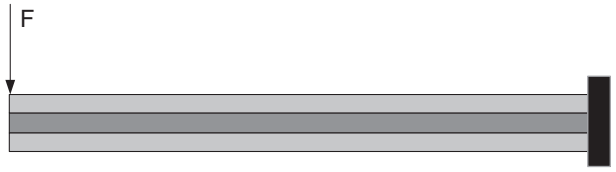

Fig. 4. Cantilever sandwich beam.

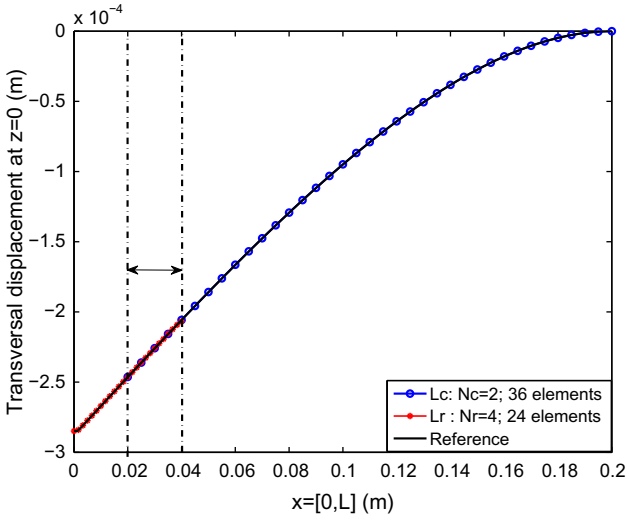

Fig. 5. Transverse displacement along the beam axis at $z=0$, two-dimensional case.

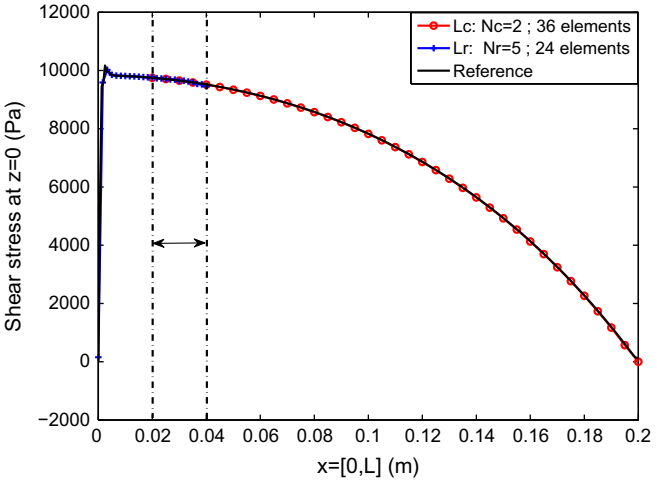

Fig. 6. Shear stress along the beam axis at $z=0$, two-dimensional case.

Table 4
Parameters of the cantilever sandwich beam.

E_f (MPa)	E_c (MPa)	ν_f, ν_c	L (m)	L_c (m)	L_r (m)	h_{tot} (m)	h_c/h_f	F (N/m)
69,000	6.9	0.3	0.2	0.18	0.04	0.01	1	100

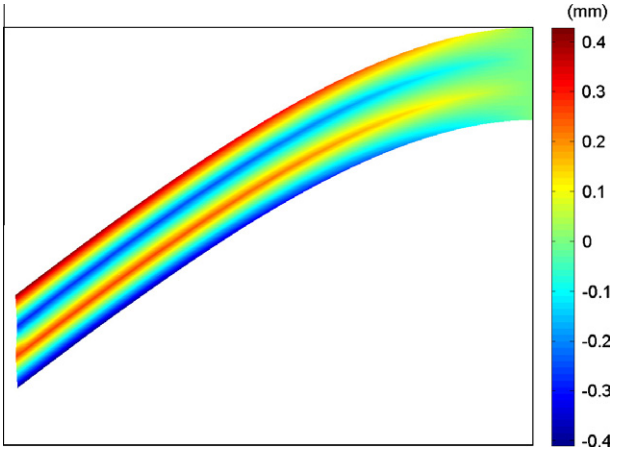

Fig. 7. Axial displacement distribution on the deformed beam.

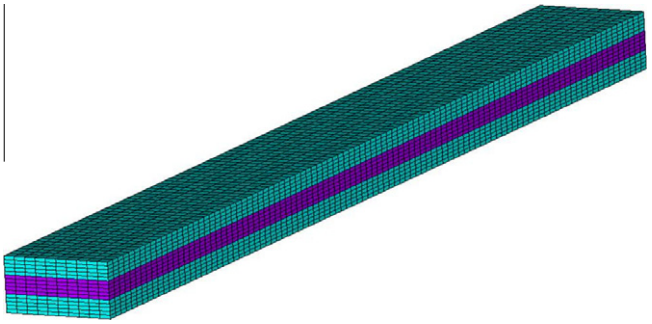

Fig. 8. The mesh of ANSYS 3D reference solution.

present the variation along the beam axis of the transverse displacement and the shear stress for $z = 0$. The CUF multi-model solution match the reference FEM solution. In particular, the local variation of the shear stress in the neighbourhood of the force is accurately predicted. The beam deformation is shown in Fig. 7. Displacement field has been multiplied by a scaling factor equal to 10^2. The effectiveness of the CVP for imposing inter-laminar congruency is verified.

4.3. Three-dimensional CUF sandwich multi-model analysis

In this subsection, we study a three-dimensional cantilever sandwich beam with width $b = 0.02$ m and a concentrated load

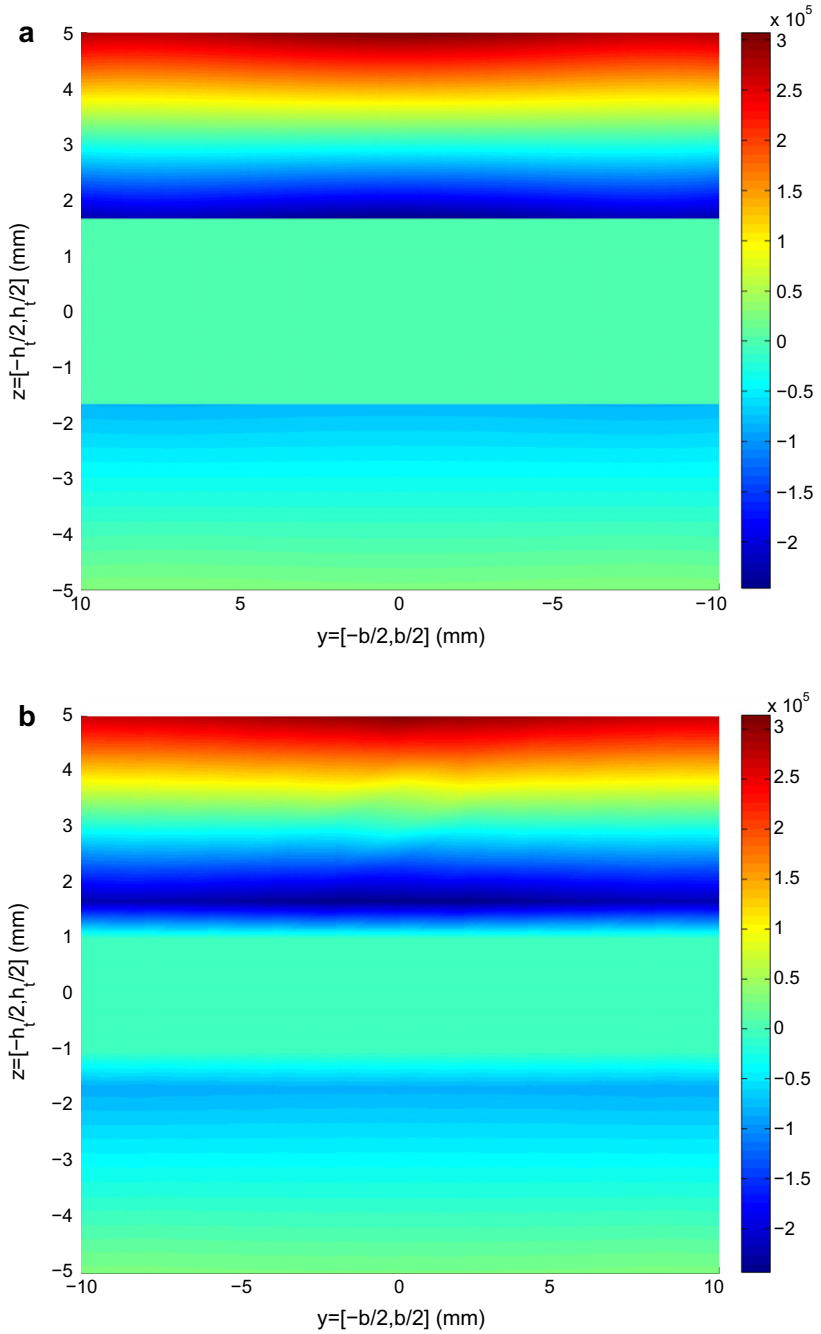

Fig. 9. Axial stress distribution at cross-section $x = 0.01$ m via (a) CUF $N_c = 2$ (36 elements) and $N_r = 5$ (24 elements) multi-model and (b) FEM 3D reference solution, three-dimensional case.

2 N applied at the point ($x = 0$, $y = 0$ and $z = h_{tot}/2$). Material properties and the other geometrical parameters can be found in Table 4. The same mesh as in the previous case has been used for the multi-model. The displacement field in the width direction is treated as the one of the transverse displacement. The three-dimensional reference solution is obtained via the commercial code ANSYS where SOLID186 quadratic element is adopted. The mesh in ANSYS is shown in Fig. 8. The distribution of the axial stress σ_{xx} above the cross-section at $x = 0.01$ m is presented in Fig. 9. The proposed multi-model solution agree with the reference one. Fig. 10 presents variation of the transverse shear stress σ_{xz} along the beam axis for $z = 0$. The proposed multi-model solution matches the reference one. In order to investigate the distribution of transverse shear stress σ_{xz} above the cross-section at $x = 0.03$ m, coarse model with length $L_c = 0.16$ m divided by 32 elements, and refined model with length $L_r = 0.5$ m discretized by 30 elements are considered. Fig. 11 shows that the proposed multi-model solution matches the reference one. The continuity of shear stress of layers' interface is not satisfied since only the displacements are assumed as a priori variables.

4.4. The computational cost comparison

In this subsection, the comparison of computational cost of each model is discussed. For example, for the sake of obtaining the convergent accurate solution of σ_{xz} distribution at $x = 0.03$ m (see Fig. 11), the required number of freedom of each model are shown respectively in Table 5. From this table, the approximate scale of computational cost is observed. It is obvious that by using multi-model, computational cost is reduced a lot compared with mono-model.

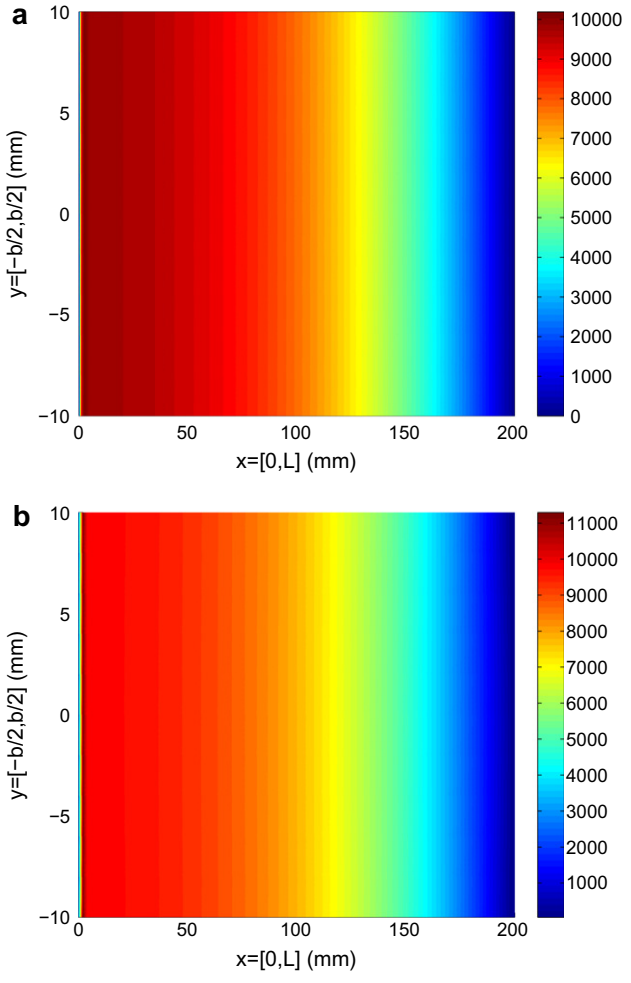

Fig. 10. Shear stress distribution along the beam axis at $z = 0$ m, via (a) CUF $N_c = 2$ (36 elements) and $N_r = 5$ (24 elements) multi-model and (b) FEM 3D reference solution, three-dimensional case.

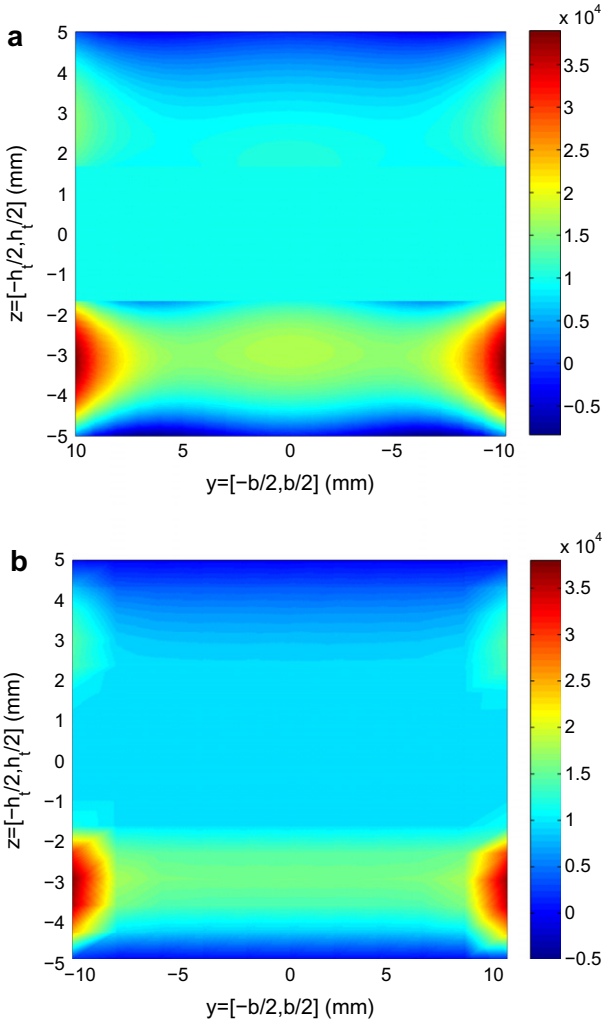

Fig. 11. Shear stress distribution at cross-section $x = 0.03$ m via (a) CUF $N_c = 2$ (32 elements) and $N_r = 5$ (30 elements) multi-model and (b) FEM 3D reference solution, three-dimensional case.

Table 5
Comparison of DOF scale of different models.

Model	ANSYS	Mono-model $N = 5$	Multi-model $N_c = 2$, $N_r = 5$
Degrees of freedom (DOF)	2.05×10^5	5.63×10^4	1.15×10^4

5. Conclusions

In the present paper, the hierarchical beam elements based on Carrera's Unified Formulation have been firstly extended to the analysis of laminated sandwich structures accounting for a layer-wise description of the displacement field. Congruency of the displacement field at core interfaces has been imposed through the Constrained Variational Principle. Multi-model solution have been,

then, derived by means of the Arlequin method. Finite elements based on different approximation order above the cross-section and with different length have been coupled in order to reduce the computational cost. Two- and three-dimensional beam models have been investigated. Results have been validated towards two- and three-dimensional FEM solution developed via the commercial code ANSYS. Numerical results have shown that the proposed CUF mono-model solution yield accurate results in the case of relatively short beams with a low ratio (as low as 10^{-4}) of the core and faces Young's moduli. The Arlequin model in the framework of CUF modelling has been proved to be effective in reducing the computational cost without loss of accuracy. Both global and local response (in the neighbourhood of the load application area) match the reference solutions.

Acknowledgments

This work has been supported by the National Natural Science Foundation of China (Grant No. 10802059) and by European FP6 MATERA Project ADYMA (FNR/MAT/08/01).

References

[1] Belouettar S, Abbadi A, Azari Z, Belouettar R, Freres P. Experimental investigation of static and fatigue behaviour of composites honeycomb materials using four point bending tests. Compos Struct 2009;87(3):265–73.
[2] Carrera E. Historical review of zig-zag theories for multilayered plates and shells. Appl Mech Rev 2003;56(3):287–308.
[3] Carrera E. Theories and finite elements for multilayered, anisotropic, composite plates and shells. Arch Comput Methods Eng 2002;9(2):87–140.
[4] Hu H, Belouettar S, Daya EM, Potier-Ferry M. Evaluation of kinematic formulations for viscoelastically damped sandwich beam modeling. J Sandwich Struct Mater 2006;8(6):477–95.
[5] Hu H, Belouettar S, Potier-Ferry M, Daya EM. Review and assessment of various theories for modelling sandwich composites. Compos Struct 2008;84(3):282–92.
[6] Lekhnitskii SG. Strength calculation of composite beams. Vestn Inzh Tekh 1935;9.
[7] Carrera E. Theories and finite elements for multilayered plates and shells: a unified compact formulation with numerical assessment and benchmarking. Arch Comput Methods Eng 2003;10(3):216–96.
[8] Carrera E, Giunta G. Refined beam theories based on a unified formulation. Int J Appl Mech 2001;2(1):117–43.
[9] Carrera E, Giunta G. Hierarchical evaluation of failure parameters in composite plates. AIAA J 2009;47(3):692–702.
[10] Carrera E, Giunta G. Exact, hierarchical solutions for localized loadings in isotropic, laminated, and sandwich shells. J Press Vessel Technol, Trans ASME 2009;131(4):0412021–04120214.
[11] Carrera E, Giunta G, Nali P, Petrolo M. Refined beam elements with arbitrary cross-section geometries. Comput Struct 2010;88(5–6):283–93.
[12] Carrera E, Giunta G, Petrolo M. A modern and compact way to formulate classical and advanced beam theories. Stirlingshire, UK: Saxe-Coburg Publications; 2010. p. 75–112 [chapter 4].
[13] Curtin WA, Miller RE. Atomistic/continuum coupling in computational materials science. Modell Simul Mater Sci Eng 2003;11(3):33–68.
[14] Liu WK, Karpov EG, Zhang S, Park HS. An introduction to computational nanomechanics and materials. Comput Methods Appl Mech Eng 2004;193(17–20):1529–78.
[15] Ben Dhia H. Multiscale mechanical problems: the Arlequin method. C R Acad Sci 1998;IIb(326):899–904.
[16] Ben Dhia H. Numerical modelling of multiscale problems: the Arlequin method. In: Proceedings of ECCM'99, München; 1999.
[17] Ben Dhia H, Rateau G. Analyse mathématique de la méthode Arlequin mixte. C R Acad Sci 2001;I(332):649–54.
[18] Ben Dhia H, Rateau G. The Arlequin method as a flexible engineering design tool. Int J Numer Methods Eng 2005;62(11):1442–62.
[19] Xiao SP, Belytschko T. A bridging domain method for coupling continua with molecular dynamics. Comput Methods Appl Mech Eng 2004;193:1645–1669.
[20] Guidault P-A, Belytschko T. Bridging domain methods for coupled atomistic-continuum models with L^2 or H^1 couplings. Int J Numer Methods Eng 2008;77(11):1566–92.
[21] Prudhomme S, Ben Dhia H, Bauman PT, Elkhodja N, Oden JT. Computational analysis of modeling error for the coupling of particle and continuum models by the Arlequin method. Comput Methods Appl Mech Eng 2008;197(41–42):3399–409.
[22] Bauman PT, Oden JT, Prudhomme S. Adaptive multiscale modeling of polymeric materials with Arlequin coupling and goals algorithms. Comput Methods Appl Mech Eng 2009;198(5–8):799–818.
[23] Hu H, Belouettar S, Potier-Ferry M, Daya EM. Multi-scale modeling of sandwich structure using the Arlequin method, part I: linear modelling. Finite Elem Anal Des 2008;45(1):37–51.
[24] Hu H, Belouettar S, Potier-Ferry M, Daya EM, Makradi A. Multi-scale nonlinear modelling of sandwich structures using the Arlequin method. Compos Struct 2010;92(2):515–22.
[25] Cochelin B, Damil N, Potier-Ferry M. Asymptotic–numerical methods and Pade approximants for non-linear elastic structures. Int J Numer Methods Eng 1994;37(7):1187–213.
[26] Zahrouni H, Cochelin B, Potier-Ferry M. Computing finite rotations of shells by an asymptotic-numerical method. Comput Methods Appl Mech Eng 1999;175(1–2):71–85.
[27] Biscani F, Giunta G, Belouettar S, Carrera E, Hu H. Variable kinematic beam elements coupled via Arlequin method. Compos Struct 2011;93(2):697–708.
[28] Reddy JN. Mechanics of laminated composite plates and shells. In: Theory and analysis. CRC Press; 2004.
[29] Reddy JN. A simple higher-order theory of laminated composite plate. J Appl Mech 1984;51(4):745–52.
[30] Touratier M. An efficient standard plate theory. Int J Eng Sci 1991;29(8):901–916.
[31] Daya EM, Potier-Ferry M. A shell element for viscoelastically damped sandwich structures. Rev Euro Élém 2002;11(1):39–56.
[32] Bauman PT, Ben Dhia H, Elkhodja N, Oden JT. On the application of the Arlequin method to the coupling of particle and continuum models. Comput Mech 2008;42:511–30.